Enhanced thermoelectric efficiency in topological insulator Bi_2Te_3 nanoplates via atomic layer deposition-based surface passivation

Jihan Chen, Jaehyun Kim, Nirakar Poudel, Bingya Hou, Lang Shen, Haotian Shi, Li Shi, and Stephen Cronin

Citation: Appl. Phys. Lett. **113**, 083904 (2018); doi: 10.1063/1.5030674
View online: https://doi.org/10.1063/1.5030674
View Table of Contents: http://aip.scitation.org/toc/apl/113/8
Published by the American Institute of Physics

Enhanced thermoelectric efficiency in topological insulator Bi_2Te_3 nanoplates via atomic layer deposition-based surface passivation

Jihan Chen,[1] Jaehyun Kim,[2] Nirakar Poudel,[1] Bingya Hou,[1] Lang Shen,[3] Haotian Shi,[4] Li Shi,[2] and Stephen Cronin[1,4,5,a)]

[1]*Ming Hsieh Department of Electrical Engineering, University of Southern California, Los Angeles, California 90089, USA*
[2]*Department of Mechanical Engineering and Texas Materials Institute, University of Texas, Austin, Texas 78712, USA*
[3]*Mork Family Department of Chemical Engineering and Materials Science, University of Southern California, Los Angeles, California 90089, USA*
[4]*Department of Chemistry, University of Southern California, Los Angeles, California 90089, USA*
[5]*Department of Physics and Astronomy, University of Southern California, Los Angeles, California 90089, USA*

(Received 24 March 2018; accepted 9 August 2018; published online 22 August 2018)

We report in-plane thermoelectric measurements of Bi_2Te_3 nanoplates, a typical topological insulator with Dirac-like metallic surface states, grown by chemical vapor deposition. The as-grown flakes exposed to ambient conditions exhibit relatively small thermopowers around $-34\,\mu$V/K due to unintentional surface doping (e.g., gas adsorption and surface oxidation). After removal of the unintentional surface doping and surface passivation by deposition of 30 nm of Al_2O_3 using atomic layer deposition (ALD), the Seebeck coefficient of these flakes increases by a factor of $5\times$ to $-169\,\mu$V/K. Here, we believe that the ALD-based surface passivation can prevent the degradation of the thermoelectric properties caused by gas adsorption and surface oxidation processes, thus, reducing the unintentional doping in the Bi_2Te_3 and increasing the Seebeck coefficient. The high surface-to-volume ratio of these thin ($\sim$10 nm thick) nanoplates make them especially sensitive to surface doping, which is a common problem among nanomaterials in general. An increase in the sample resistance is also observed after the ALD process, which is consistent with the decrease in doping. *Published by AIP Publishing*. https://doi.org/10.1063/1.5030674

The potential use of nanoscale materials to enhance the thermoelectric properties of energy conversion dates back to the theoretical predictions of Hicks and Dresselhaus in 1994.[1,2] Mechanisms of enhancement include increased density of electronic states in low dimensions,[3] increased phonon scattering,[4] and quantum confinement-induced band gap engineering.[5] However, in practice, reducing materials and devices to low dimensions (or nanoscale dimensions) often presents deleterious effects associated with poor electrical contacts,[6] surface depletion,[7,8] and unintentional doping,[9] which are not important in bulk material systems. For example, the thermoelectric performance of monolayer MoS_2 varies more widely than bulk MoS_2.[10–12] In fact, nanoscale forms of Bi_2Te_3 typically have lower ZT values that their bulk counterparts due to these issues.[13–15]

Oxygen plasma treatment of 2D materials has been shown to improve the materials properties, through the remediation of unintentional doping. Dhall *et al.* shows a 16-fold increase in the luminescence efficiency of MoS_2 after exposure to a brief oxygen plasma and a shift in the threshold voltage of as much as 18 V in MoS_2-based field effect transistors.[9,16] Javey's group reported an air-stable, solution-based chemical treatment using an organic non-oxidizing superacid [bis(trifluoromethane) sulfonimide (TFSI)], which uniformly enhances the photoluminescence and minority carrier lifetime of MoS_2 monolayers by more than two orders of magnitude.[17] Pettes *et al.* explored the effects of surface band bending and scattering on thermoelectric transport in suspended bismuth telluride nanoplates using microfabricated heaters and thermometers.[18] They saw the direct effect of surface scattering and surface doping as a function of Bi_2Te_3 nanoplate thickness. They also reported that both chemical alloying and surface potential modification can play important roles in optimizing the thermoelectric properties in ultrathin $(Bi_{1-x}Sb_x)_2Te_3$ nanoplates as well.[19] In the work presented here, we report a facile method to improve the thermoelectric efficiency of Bi_2Te_3 nanoplates through remediation of unintentional surface doping.

In this work, two dimensional (2D) single crystal nanoplates (NPs) of bismuth telluride were synthesized by a catalyst-free vapor-solid method following an approach similar to that of Kong *et al.*[20] Bulk Bi_2Te_3 was placed in the center of a 1 inch fused quartz tube in a hot wall furnace, and silicon substrates coated with 280 nm thermally grown SiO_2 were placed approximately 10–14 inches downstream. The quartz tube was evacuated with a mechanical pump, and then the temperature was slowly ramped (1–2 °C min^{-1}) to 450–480 °C under flowing Ar. The pressure was maintained in the range of 20–70 Torr for the duration of the synthesis before slowly cooling back to room temperature. Typical resultant 2D crystals are hexagonal or triangular in shape with sizes on the order of 2–50 μm and uniform thicknesses of 3–50 nm. Flakes are then transferred to an oxidized silicon wafer using a home built transfer setup consisting of a sharp

a)Author to whom correspondence should be addressed: scronin@usc.edu

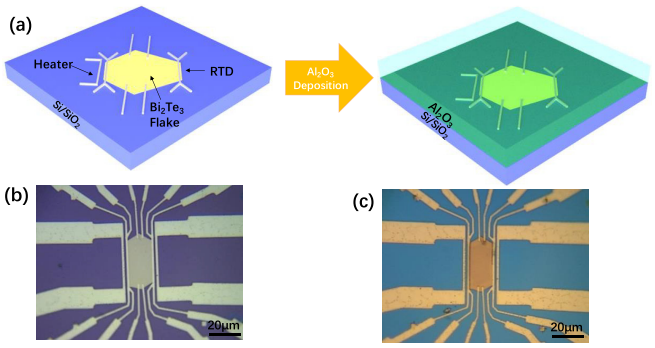

FIG. 1. Schematic diagram of the device fabrication process (a) and optical image of the device before (b) and after (c) Al_2O_3 deposition.

tungsten tip to transfer the nanoplate from the growth substrate to the device substrate. Top electrodes, heaters, and 4-probe resistance thermometers (RTDs) are then patterned using electron beam lithography followed by metal deposition of Au, as shown in Fig. 1. Optical microscope images of the sample before and after Al_2O_3 deposition are shown in Fig. 1. Before 30 nm Al_2O_3 atomic layer deposition (ALD) deposition, fabricated devices are immersed into buffered hydrochloric acid (HCl) to remove the native oxide and surface adsorbates. For 10:1 HCl, the typical etching rate of oxide is 23 nm/min. We expect that our 4-s HCl dip is just enough to etch away the 1–2 nm native oxide, while having a minimal impact on the thickness of the Bi_2Te_3 flake. This acid dip is followed immediately by an evaporation of 1 nm Al passivation, which improves the nucleation of the ALD layer. After the ALD process, a clear contrast can be seen in the Bi_2Te_3 nanoplate after the ALD process. Interestingly, there is no change observed in the Raman spectra, as shown in Fig. S1 of the supplementary material, indicating that there is no significant change in the lattice structure after the ALD process. The resistance vs. temperature relation of each 4-probe RTD is calibrated in a temperature-controlled (Linkam) stage before and after depositing Al_2O_3, as shown in Fig. 2. The RTD resistance (40 Ω) is two orders magnitude smaller than the in-plane resistance of the Bi_2Te_3 nanoplate (8 kΩ), ensuring that there is negligible current leakage in and out of the Bi_2Te_3 nanoplates from the metal thermometer line.

Figure 3 shows the thermoelectric voltage plotted as a function of the temperature gradient measured from the Bi_2Te_3 nanoplate shown in Fig. 1. Before Al_2O_3 deposition, the Seebeck coefficient of this flake was −34.3 μV/K. Here, the two datasets plotted in the figure correspond to positive and negative voltages applied to the heater. After ALD, the Seebeck coefficient increases to −168.9 μV/K, which is a factor of 5× increase. We also observe a factor of 13× increase in the 4-probe resistance of the nanoplate, which is consistent with a decrease in the unintentional doping of this material. Together, this corresponds to a twofold increase in the power factor (i.e., $S^2\sigma$) of the Bi_2Te_3 nanoplates with a value of 0.434 mW/m·K^2. The value is approximately one order of magnitude below bulk values for Bi_2Te_3 alloys.[21]

Figure 4 shows the results of Hall effect measurements plotted as a function of temperature of the Bi_2Te_3 nanoplate before and after Al_2O_3 deposition. An optical microscope image of the device is shown in Fig. 4(a). Hall carrier densities plotted as a function of temperature before and after ALD are shown in Fig. 4(b). In comparison, after the ALD-based surface passivation, the carrier concentration is approximately 40% lower than before, which indicates that the difference of the carrier concentrations arises from the unintentional n-type surface doping caused by the exposure to ambient conditions.

Figure S6 of the supplementary material shows the results of similar thermoelectric measurements performed on a different Bi_2Te_3 nanoplate sample. Here, we observe a similar change in the optical contrast of the material after the ALD process, as evident in Fig. S2. Here, the Seebeck coefficient of the as-grown Bi_2Te_3 nanoplate is −30.1 μV/K,

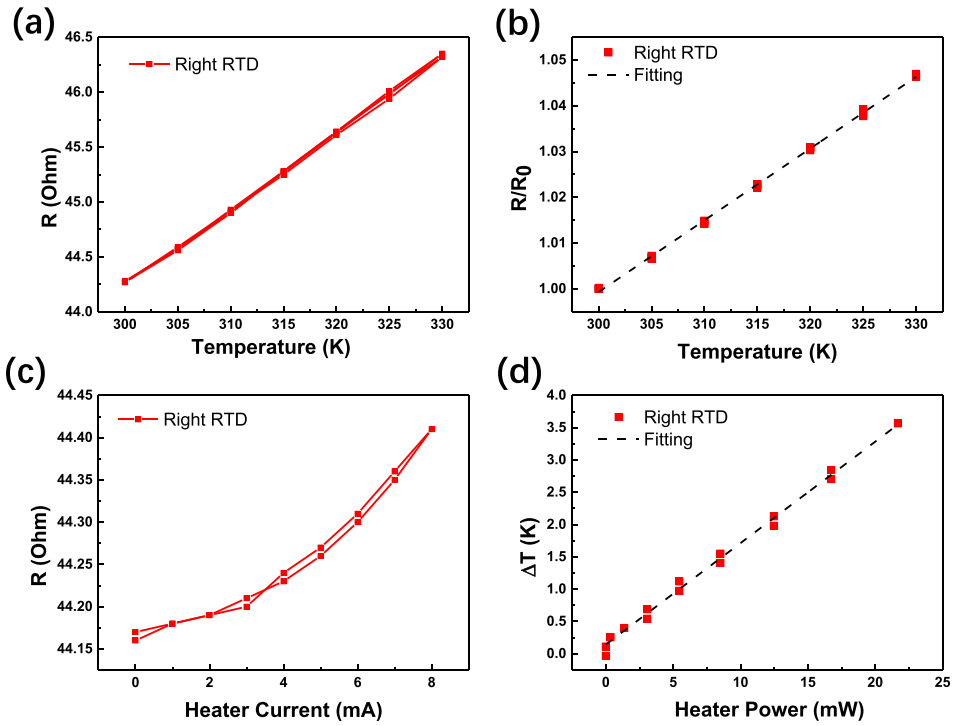

FIG. 2. Temperature calibration of the right metal RTD of the Bi_2Te_3 device shown in Fig. 1. (a) The resistance of the RTD measured at different temperatures. (b) Normalized resistance (R/R_0, R_0 is the resistance at 300 K) plotted as a function of T. (c) The resistance change of the RTDs under various heating currents. (d) Temperature change of the metal RTDs plotted as a function of heating power.

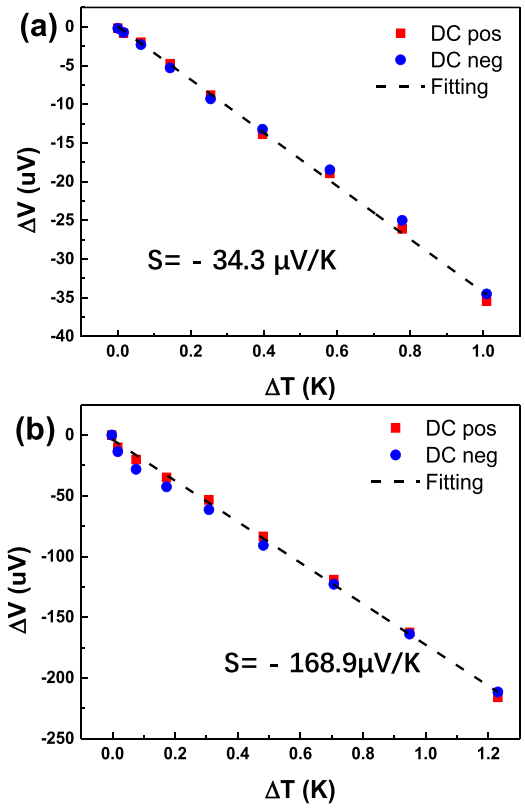

FIG. 3. In-plane Seebeck coefficient of the Bi_2Te_3 flake (a) before and (b) after Al_2O_3 deposition.

which increases by 4.8-fold to $-145.7\,\mu V/K$ after Al_2O_3 deposition. These results confirm that the effects observed in Fig. 3 are roust and repeatable. Again, we observe a 11-fold increase in the 4-probe resistance of the samples after the ALD process, corresponding to a net increase in the power factor of twofold. In our previous work, we have used a two-channel model to analyze the carrier concentration dependence of the Seebeck coefficient and electrical conductivity.[18] Based on this model, we estimate a change in the Fermi energy of approximately 50–100 meV due to the atomic layer deposition process.

As a prototypical topological insulator, Bi_2Te_3 has the same unconventional band structures as other topological insulators (TIs) that have an insulating bulk band gap and metallic surface state, which consists of a single Dirac cone. Thus, the topological surface state (TSS) plays an important role in transport measurements of Bi_2Te_3 nanoplates and the modification of the TSS have been reported during the past decade. Chen *et al*. have shown a strong n-type doping of the surface state of Bi_2Te_3 after an exposure to air at room temperature.[22] The formation of two-dimensional quantum well states have also been observed near the exposed surface of the Bi_2Te_3. In the work of Benia *et al*., topological insulator Bi_2Se_3 was exposed to water vapor and results in a band bending that shifts the Dirac point deep into the occupied states and quantum well states were created as well.[23] The work of Pettes *et al*., reported that pronounced n-type surface band bending can yield a suppressed and even negative Seebeck coefficient in unintentionally p-type doped Bi_2Te_3 nanoplates.[17] Liu and Ye have shown that the proper selection of ALD precursors play a critical role in device performance of Bi_2Te_3 based TI field-effect transistors. As precursors, H_2O creates much weaker surface damage than ozone during the first several cycles of ALD growth since ozone is a stronger oxidant than H_2O.[24] To minimize the surface damage from precursor, we use TMA/H_2O as precursors for our ALD process. In the work presented here, before the surface passivation, our Bi_2Te_3 nanoplates exposed to ambient air have a native oxide and gas adsorption on the surface, which leads to n-type surface band bending, which is consistent with the negative Seebeck coefficient ($-34.3\,\mu V/K$). We believe that after the removal of surface doping, ALD-based surface passivation provides an effective way to preserve the TSS from environmental degradation, presenting a possible mechanism for "TSS protection," thus inhibiting the effects of unintentional doping in the nanomaterial. This accounts for both the marked increase Seebeck coefficient and increase in sample resistance.

In summary, we report in-plane thermoelectric measurements of Bi_2Te_3 nanoplates grown by chemical vapor deposition (CVD). The as-grown flakes exhibit relatively small thermopowers around $-34\,\mu V/K$, due to unintentional surface doping, likely due to gas adsorption and surface oxidation. After removal of the surface doping in a buffered HCl solution, and 1 nm Al passivation followed by a deposition of 30 nm of Al_2O_3 using atomic layer deposition (ALD), the Seebeck coefficient of these flakes increases by a factor of $5\times$ to $-169\,\mu V/K$. Here, we believe that the ALD-based surface passivation can effectively reveal the topological surface states of Bi_2Te_3 nanoplates by inhibiting n-type surface band bending, which is caused by environmental exposure, thus preventing unintentional doping in the Bi_2Te_3 and thereby increasing the Seebeck coefficient. The high surface-to-volume ratio of these thin (~10 nm thick) nanoplates makes them especially sensitive to surface doping and nanomaterials in general. An increase in the sample resistance is also observed after the ALD process, which is consistent with the decrease in doping.

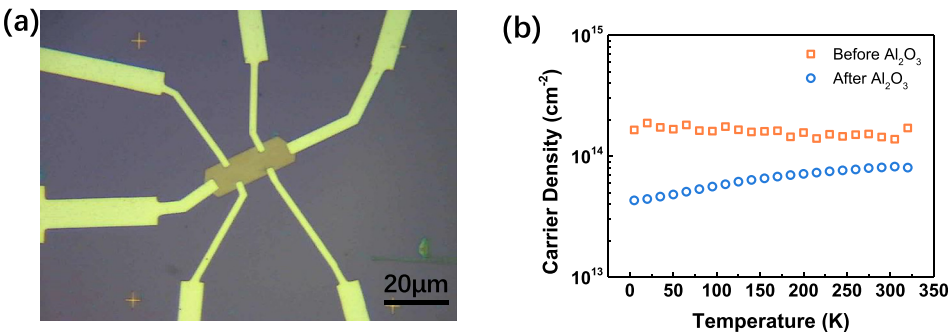

FIG. 4. Hall measurements of the Bi_2Te_3 flake. (a) Optical microscope image of the device and (b) Hall carrier densities of the Bi_2Te_3 flake before and after Al_2O_3 deposition.

See supplementary material for the details of the Raman spectroscopy of Bi_2Te_3 sample before and after ALD passivation, Seebeck measurement for the second Bi_2Te_3 sample, and the Transmission Electron Microscope (TEM) Energy Dispersive Spectroscopy (EDS) analysis.

This research was supported by the Department of Energy (DOE) Award Nos. DE-FG02-07ER46376 (J.C.), DE-FG02-07ER46377 (J.K. and L.S.), and NSF Award No. 1402906 (N.P.).

[1]L. D. Hicks and M. S. Dresselhaus, "Effect of quantum-well structures on the thermoelectric figure of merit," Phys. Rev. B **47**(19), 12727–12731 (1993).
[2]L. D. Hicks and M. S. Dresselhaus, "Thermoelectric figure of merit of a one-dimensional conductor," Phys. Rev. B **47**(24), 16631–16634 (1993).
[3]M. S. Dresselhaus, G. Dresselhaus, X. Sun, Z. Zhang, S. B. Cronin, and T. Koga, "Low-dimensional thermoelectric materials," Phys. Solid State **41**(5), 679–682 (1999).
[4]D. G. Cahill, W. K. Ford, K. E. Goodson, G. D. Mahan, A. Majumdar, H. J. Maris, R. Merlin, and S. Phillpot, "Nanoscale thermal transport," J. Appl. Phys. **93**(2), 793–818 (2003).
[5]T. Koga, X. Sun, S. B. Cronin, and M. S. Dresselhaus, "Carrier pocket engineering to design superior thermoelectric materials using GaAs/AlAs superlattices," Appl. Phys. Lett. **73**(20), 2950–2952 (1998).
[6]S. B. Cronin, Y. M. Lin, O. Rabin, M. R. Black, J. Y. Ying, M. S. Dresselhaus, P. L. Gai, J. P. Minet, and J. P. Issi, "Making electrical contacts to nanowires with a thick oxide coating," Nanotechnology **13**(5), 653–658 (2002).
[7]S. Arab, M. Yao, P. Anderson, M. Povinelli, C. Zhou, P. D. Dapkus, and S. B. Cronin, "Enhanced Fabry-Perot resonance in GaAs nanowires through surface passivation and local field enhancement," Nano Res. **7**, 1146–1153 (2014).
[8]S. Arab, C. Chi, T. Shi, Y. Wang, D. P. Dapkus, H. E. Jackson, L. M. Smith, and S. B. Cronin, "Effects of surface passivation on twin-free GaAs nanosheets," ACS Nano **9**, 1336–1340 (2015).
[9]R. Dhall, Z. Li, E. Kosmowska, and S. B. Cronin, "Charge neutral MoS_2 field effect transistors through oxygen plasma treatment," J. Appl. Phys. **120**(19), 195702 (2016).
[10]S. Bhattacharyya, T. Pandey, and A. K. Singh, "Effect of strain on electronic and thermoelectric properties of few layers to bulk MoS_2," Nanotechnology **25**(46), 465701 (2014).
[11]S. Kumar and U. Schwingenschlögl, "Thermoelectric response of bulk and monolayer $MoSe_2$ and WSe_2," Chem. Mater. **27**(4), 1278–1284 (2015).
[12]M. Kayyalha, J. Maassen, M. Lundstrom, L. Shi, and Y. P. Chen, "Gate-tunable and thickness-dependent electronic and thermoelectric transport in few-layer MoS_2," J. Appl. Phys. **120**(13), 134305 (2016).
[13]J. Zhou, C. Jin, J. H. Seol, X. Li, and L. Shi, "Thermoelectric properties of individual electrodeposited bismuth telluride nanowires," Appl. Phys. Lett. **87**(13), 133109 (2005).
[14]A. Mavrokefalos, A. L. Moore, M. T. Pettes, L. Shi, W. Wang, and X. Li, "Thermoelectric and structural characterizations of individual electrodeposited bismuth telluride nanowires," J. Appl. Phys. **105**(10), 104318 (2009).
[15]B. Hamdou, J. Kimling, A. Dorn, E. Pippel, R. Rostek, P. Woias, and K. Nielsch, "Thermoelectric characterization of bismuth telluride nanowires, synthesized via catalytic growth and post-annealing," Adv. Mater. **25**(2), 239–244 (2013).
[16]R. Dhall, M. R. Neupane, D. Wickramaratne, M. Mecklenburg, Z. Li, C. Moore, R. K. Lake, and S. Cronin, "Direct bandgap transition in many-layer MoS_2 by plasma-induced layer decoupling," Adv. Mater. **27**(9), 1573 (2015).
[17]M. Amani, D.-H. Lien, D. Kiriya, J. Xiao, A. Azcatl, J. Noh, S. R. Madhvapathy, R. Addou, S. KC, M. Dubey, K. Cho, R. M. Wallace, S.-C. Lee, J.-H. He, J. W. Ager III, X. Zhang, E. Yablonovitch, and A. Javey, "Near-unity photoluminescence quantum yield in MoS_2," Science **350**, 1065 (2015).
[18]M. T. Pettes, J. Maassen, I. Jo, M. S. Lundstrom, and L. Shi, "Effects of surface band bending and scattering on thermoelectric transport in suspended bismuth telluride nanoplates," Nano Lett. **13**(11), 5316–5322 (2013).
[19]M. T. Pettes, J. Kim, W. Wu, K. C. Bustillo, and L. Shi, "Thermoelectric transport in surface- and antimony-doped bismuth telluride nanoplates," APL Mater. **4**(10), 104810 (2016).
[20]D. Kong, W. Dang, J. J. Cha, H. Li, S. Meister, H. Peng, Z. Liu, and Y. Cui, "Few-layer nanoplates of Bi_2Se_3 and Bi_2Te_3 with highly tunable chemical potential," Nano Lett. **10**(6), 2245–2250 (2010).
[21]D. Li, R.-R. Sun, and X.-Y. Qin, "Improving thermoelectric properties of p-type Bi_2Te_3-based alloys by spark plasma sintering," Prog. Nat. Sci.: Mater. Int. **21**(4), 336–340 (2011).
[22]C. Chen, S. He, H. Weng, W. Zhang, L. Zhao, H. Liu, X. Jia, D. Mou, S. Liu, J. He, Y. Peng, Y. Feng, Z. Xie, G. Liu, X. Dong, J. Zhang, X. Wang, Q. Peng, Z. Wang, S. Zhang, F. Yang, C. Chen, Z. Xu, X. Dai, Z. Fang, and X. J. Zhou, "Robustness of topological order and formation of quantum well states in topological insulators exposed to ambient environment," Proc. Natl. Acad. Sci. U. S. A. **109**(10), 3694–3698 (2012).
[23]H. M. Benia, C. Lin, K. Kern, and C. R. Ast, "Reactive chemical doping of the Bi_2Se_3 topological insulator," Phys. Rev. Lett. **107**(17), 177602 (2011).
[24]H. Liu and P. D. Ye, "Atomic-layer-deposited Al_2O_3 on Bi_2Te_3 for topological insulator field-effect transistors," Appl. Phys. Lett. **99**(5), 052108 (2011).